AGU PUBLICATIONS

JGR

Journal of Geophysical Research: Solid Earth

RESEARCH ARTICLE
10.1002/2014JB011776

This article is a companion to *Bevilacqu et al.* [2015] doi:10.1002/2014JB011775.

Key Points:
- Probabilistic invasion maps for PDC were produced
- Maps considered the variability of vent location, eruptive scale, and topography
- The effect of some key uncertainties was quantified

Supporting Information:
- Text S1
- Data Set S1
- Data Set S2
- Data Set S3

Correspondence to:
A. Neri,
augusto.neri@ingv.it

Citation:
Neri, A., et al. (2015), Quantifying volcanic hazard at Campi Flegrei caldera (Italy) with uncertainty assessment: 2. Pyroclastic density current invasion maps, *J. Geophys. Res. Solid Earth*, *120*, 2330–2349, doi:10.1002/2014JB011776.

Received 23 NOV 2014
Accepted 13 MAR 2015
Accepted article online 19 MAR 2015
Published online 22 APR 2015

Quantifying volcanic hazard at Campi Flegrei caldera (Italy) with uncertainty assessment: 2. Pyroclastic density current invasion maps

Augusto Neri[1], Andrea Bevilacqua[1,2], Tomaso Esposti Ongaro[1], Roberto Isaia[3], Willy P. Aspinall[4,5], Marina Bisson[1], Franco Flandoli[6], Peter J. Baxter[7], Antonella Bertagnini[1], Enrico Iannuzzi[3], Simone Orsucci[1,8], Marco Pistolesi[9,10], Mauro Rosi[10,11], and Stefano Vitale[12]

[1]Istituto Nazionale di Geofisica e Vulcanologia, Sezione di Pisa, Pisa, Italy, [2]Scuola Normale Superiore, Pisa, Italy, [3]Osservatorio Vesuviano, Istituto Nazionale di Geofisica e Vulcanologia, Naples, Italy, [4]School of Earth Sciences, University of Bristol, Bristol, UK, [5]Aspinall and Associates, Tisbury, UK, [6]Dipartimento di Matematica, Università di Pisa, Pisa, Italy, [7]Institute of Public Health, University of Cambridge, Cambridge, UK, [8]Dipartimento di Fisica, Università di Pisa, Pisa, Italy, [9]Dipartimento di Scienze della Terra, Università di Firenze, Florence, Italy, [10]Dipartimento di Scienze della Terra, Università di Pisa, Pisa, Italy, [11]Dipartimento della Protezione Civile, Rome, Italy, [12]Dipartimento di Scienze della Terra, dell'Ambiente e delle Risorse, Università di Napoli Federico II, Naples, Italy

Abstract Campi Flegrei (CF) is an example of an active caldera containing densely populated settlements at very high risk of pyroclastic density currents (PDCs). We present here an innovative method for assessing background spatial PDC hazard in a caldera setting with probabilistic invasion maps conditional on the occurrence of an explosive event. The method encompasses the probabilistic assessment of potential vent opening positions, derived in the companion paper, combined with inferences about the spatial density distribution of PDC invasion areas from a simplified flow model, informed by reconstruction of deposits from eruptions in the last 15 ka. The flow model describes the PDC kinematics and accounts for main effects of topography on flow propagation. Structured expert elicitation is used to incorporate certain sources of epistemic uncertainty, and a Monte Carlo approach is adopted to produce a set of probabilistic hazard maps for the whole CF area. Our findings show that, in case of eruption, almost the entire caldera is exposed to invasion with a mean probability of at least 5%, with peaks greater than 50% in some central areas. Some areas outside the caldera are also exposed to this danger, with mean probabilities of invasion of the order of 5–10%. Our analysis suggests that these probability estimates have location-specific uncertainties which can be substantial. The results prove to be robust with respect to alternative elicitation models and allow the influence on hazard mapping of different sources of uncertainty, and of theoretical and numerical assumptions, to be quantified.

1. Introduction

Campi Flegrei (CF) is an example of a densely populated and active caldera characterized by predominantly explosive eruptive activity [*Rosi et al.*, 1983; *Orsi et al.*, 2004; *Smith et al.*, 2011]. Eruptions started more than 80 ka B.P., included the two large caldera collapse events: the Campanian Ignimbrite (CI) and the Neapolitan Yellow Tuff (NYT) eruptions, and continued over the last 15 ka through three main cycles of activity. These lasted from several centuries to a few millennia each, alternated by periods of quiescence of several millennia [*Orsi et al.*, 2004; *Smith et al.*, 2011]. Key features of this activity have been eruptions from different vents scattered within the caldera, with individual events spanning a large range of eruptive scales. The products of the explosive activity can be found over most of the Campanian region in conspicuous pyroclastic deposits generated by tephra fallout and pyroclastic density currents (PDCs). PDCs represent the main hazard of this volcanic system [*Rosi et al.*, 1983; *Di Vito et al.*, 1999; *Orsi et al.*, 2004]. Due to their velocity, temperature, and particle concentrations, PDCs can produce heavy damage to urban structures and lethal conditions for human beings [*Baxter et al.*, 2005; *Neri et al.*, 2014]. Given the very high urbanization of the caldera itself and its proximity to the city of Naples, it is of prime importance that areas which may potentially be affected by PDCs are identified and ranked in terms of exposure likelihood in order that civil authorities can prepare suitable mitigation measures [e.g., *Baxter et al.*, 2008; *Neri et al.*, 2008].

Basic mapping of PDC hazard at CF has been already reported in previous studies. Some related to field reconstruction and numerical modeling of specific past events of CF, while others endeavored to produce

specific or integrated PDC hazard maps in which variabilities of important parameters of the volcanic system, such as the eruption scale and vent location, were explicitly accounted for. For instance, *Lirer et al*. [2001] reconstructed the distribution of PDC deposits from the main events of the last 5 ka and outlined a zonation of areas potentially affected by PDCs. Similarly, *Orsi et al*. [2004] used field data to reconstruct the distribution of deposits in the last 15 ka and proposed a qualitative PDC hazard invasion map based on the last 5 ka of activity. In both studies, the eastern part of the caldera was found to have the greatest hazard exposure; however, the area considered for PDCs was limited to that within the caldera rim (i.e., excluding the Collina di Posillipo). *Rossano et al*. [2004] proposed a hazard map based on a dynamic 1-D Bingham flow model, which considered the variability of eruptive scale (including very large caldera collapse events) and assumed a uniform vent opening probability in an area centered on the town of Pozzuoli. *Todesco et al*. [2006] and *Esposti Ongaro et al*. [2008a], using 2-D and 3-D numerical multiphase flow simulations of Plinian type events, analyzed in more detail the propagation dynamics of PDCs within the caldera to improve the description of the complex interaction between flows and topography. Those studies were focused specifically on the eastern sector of the caldera and showed that, for some positions of the vent, PDC flows could overtop Collina di Posillipo, a notable topographical barrier for the central part of the city of Naples.

More recently, *Alberico et al*. [2011], starting from the probability distribution of new vent opening positions of *Alberico et al*. [2002] and the occurrence probabilities of the three eruption size categories of the last 5 ka, as defined by *Orsi et al*. [2009], produced a qualitative integrated hazard map of PDC invasion for the city of Naples with five levels of hazard (Vesuvius hazards were also included in the map). Similar maps, this time associated with various eruption VEIs (volcanic explosivity index), were also proposed by *Alberico et al*. [2002]. For both studies, the invasion areas were determined using the energy cone model based on the assumption of linear decay of flow energy with distance [*Hsu*, 1975]. In both cases, the final invasion maps were only qualitative and did not account for any epistemic uncertainty quantification associated with the properties of the volcanic system and its modes and dynamics of eruption.

Where probabilities are associated with them, the above maps represent background, or long-term/base-rate, assessments of PDC hazard in the sense that none of them take into account information and measurements that would come from monitoring and observation networks during an unrest or eruptive episode. This context is necessary because of the present difficulty of predicting the timing, size, and vent location of a future eruption, based on current understanding of the state of the volcano and monitoring data. As a consequence, the definition of a quantitative background probabilistic PDC invasion map is a fundamental need not only for the aim of effective urban planning for risk mitigation but also to have an a priori probabilistic spatial distribution of hazard to be updated during the crisis [see, for instance, *Marzocchi and Woo*, 2009; *Spiller et al*., 2014; *Wadge and Aspinall*, 2014].

The present study focuses on the definition of quantitative probabilistic PDC invasion hazard maps for the CF area, incorporating key-controlling, but uncertain, variables of the system, particularly vent location and eruptive scale of future activity. Probabilistic maps conditional on the occurrence of an explosive eruption are produced by a Monte Carlo simulation approach, using a simplified invasion model able to represent main topographic effects. In addition, our mapping attempts to quantify, by using a formal structured expert elicitation approach, some of the main sources of epistemic uncertainty, such as the location of future vent opening [*Bevilacqua et al*., 2015], the reconstruction of the dispersal of PDC deposits, and the possibility that a future eruption could be characterized by the opening of two simultaneous vents located perhaps several kilometers apart, as highlighted by *Isaia et al*. [2009] for the Averno 2 and Solfatara eruptions. We first present our methods, followed by descriptions of the main data sets, the modeling tools, and the resulting hazard maps.

2. Methods

Our mapping work integrates information on the distribution of the spatial probability of vent opening, the density distribution of areas previously invaded by PDCs, and the results from a simplified PDC flow invasion model. It is very difficult to predict the exact location of the next active vent as well as the scale (or typology) of the next eruptive event, so this imposes the requirement to consider the potential physical variability of these factors when producing hazard maps. Moreover, much of the available information is

conditioned by large epistemic uncertainties that significantly influence the resulting maps. As in the companion paper [*Bevilacqua et al.*, 2015], we implemented a doubly stochastic model able to explicitly consider, in addition to the aleatoric variability of the process, some of the main uncertainties by using structured expert elicitation techniques [*Cooke*, 1991; *Aspinall*, 2006]. Such methods allow uncertainty distributions on identified variables to be determined for hazard assessment purposes, based on expert judgment when insufficient data or incomplete knowledge of the system do not permit conventional statistical enumeration of uncertainties (see *Bevilacqua et al.* [2015], Appendix A, for a more detailed description of the approach used).

2.1. Probabilistic Spatial Distribution of Vent Opening

We start with the information on the probabilistic spatial distribution of vent opening location (also called susceptibility map, e.g., *Martì and Felpeto* [2010]) derived from the analysis presented in the companion paper [*Bevilacqua et al.*, 2015]. In that analysis it was assumed that the probability map of new vent opening over the caldera, conditional on the occurrence of an eruption, could be expressed as a linear combination of the distribution of the eruptive vents that opened during the three epochs of recent activity of the volcano (i.e., the last 15 ka), the distributions of maximum fault displacement, and surface fracture density. In addition, it was considered that the probability of new intracaldera vent opening could possibly be correlated to other variables or unidentified processes which, in this phase of our investigation, cannot be included specifically: to accommodate the influence of such unknowns, a single compensating surrogate contribution was added, assumed uniformly distributed inside the Neapolitan Yellow Tuff caldera.

The analysis in *Bevilacqua et al.* [2015] also quantified the influence of some of the main sources of epistemic uncertainty that affect the hazard distribution. In particular, their analysis considered the uncertain localization of eruptive vents as reconstructed from field data, the number of past events which do not correspond to presently identified vents but for which stratigraphic evidence exists (i.e., "lost vents"), and also the uncertain weights to be associated with variables that contribute to the definition of the vent opening map. For the definition of these weights, as well as of other relevant uncertain parameterizations, the analysis used expert judgment techniques [*Aspinall*, 2006], with a simple logic tree of target questions and various complementary procedures of structured elicitation to test the sensitivity of uncertainty quantifications to the different models [e.g., *Cooke*, 1991; *Flandoli et al*., 2011].

Figure 1 shows an example of vent opening probability maps obtained with the above procedure [*Bevilacqua et al.*, 2015]. The three maps (Figures 1a–1c) represent, respectively, the 5th percentile, the mean, and the 95th percentile of the uncertainty distribution of the vent opening location map. The distribution of past vents was computed by assuming a partitioning of the caldera into 16 homogeneous zones, with uniform spatial distributions within each. However, very similar maps were also generated by computing a distribution of past vent positions based on Gaussian kernel functions. These synthesized results show the presence of a high-probability region of vent opening in the central eastern part of the caldera (i.e., the Astroni-Agnano-Solfatara area), whereas the rest of the caldera is characterized by significantly lower probability values with local secondary maxima in the Soccavo and Pisani plains and in the western zones of Averno-Monte Nuovo-Baia-Capo Miseno.

2.2. Distribution of PDC Invasion Areas

Limitations in our ability to predict the type and scale of the next eruption event require a hazard mapping approach that considers a range of possible eruptive scenarios. We take the well-known history of eruptive activity from the last 15 ka and assume that it will be representative of future patterns of behavior of the volcano. Very large scale eruptions (i.e., caldera forming), such as the NYT and the CI, are not included in the data set due to their very low probability of occurrence (well below 1% based on frequency of occurrence estimates [e.g., *Rosi et al*., 1983; *Orsi et al*., 2004]).

We designated the areas invaded by PDCs as a random variable representative of the aleatoric variability affecting the next eruption event scale. The parameters of this variable were then assumed to be affected by some epistemic uncertainty as described in the following. The PDC invasion model allows us to use the area invaded by the flow as an input. The data set on areas inundated by PDCs that occurred in the three epochs of activity (plus Monte Nuovo) largely relies on the work of *Orsi et al.* [2004], with a few minor modifications and updates due to the most recent research findings (Figure 2). In detail, 20 records were included for Epoch I, 6 for

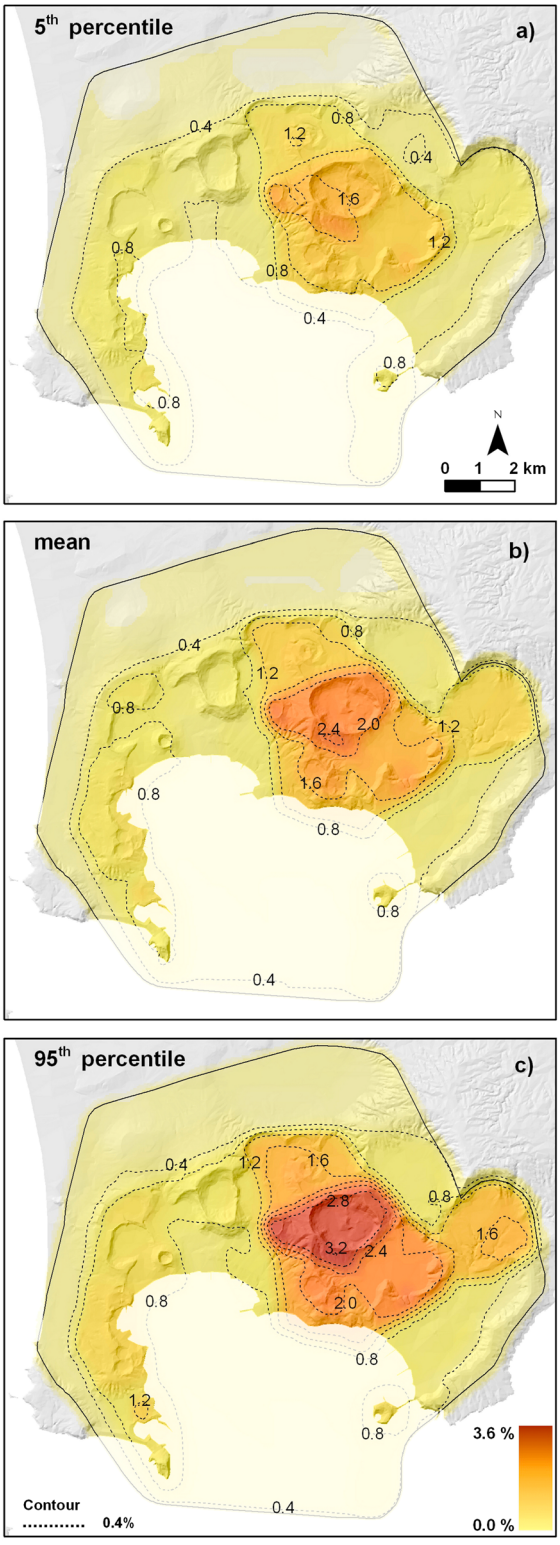

Figure 1. Probability maps of new vent opening location obtained from *Bevilacqua et al.* [2015]. Contours and colors indicate the percentage probability of vent opening per km^2 conditional on the occurrence of an eruption. (a) The 5th percentile, (b) mean, and (c) 95th percentile values. The maps were created by using a partition of the caldera into 16 homogeneous zones in order to compute the density of past vents; similar distributions were obtained by using kernel functions (see *Bevilacqua et al.* [2015], for further explanations). Note that for the definition of the PDC invasion maps we do not consider the offshore portion of the caldera as a possible area of vent opening.

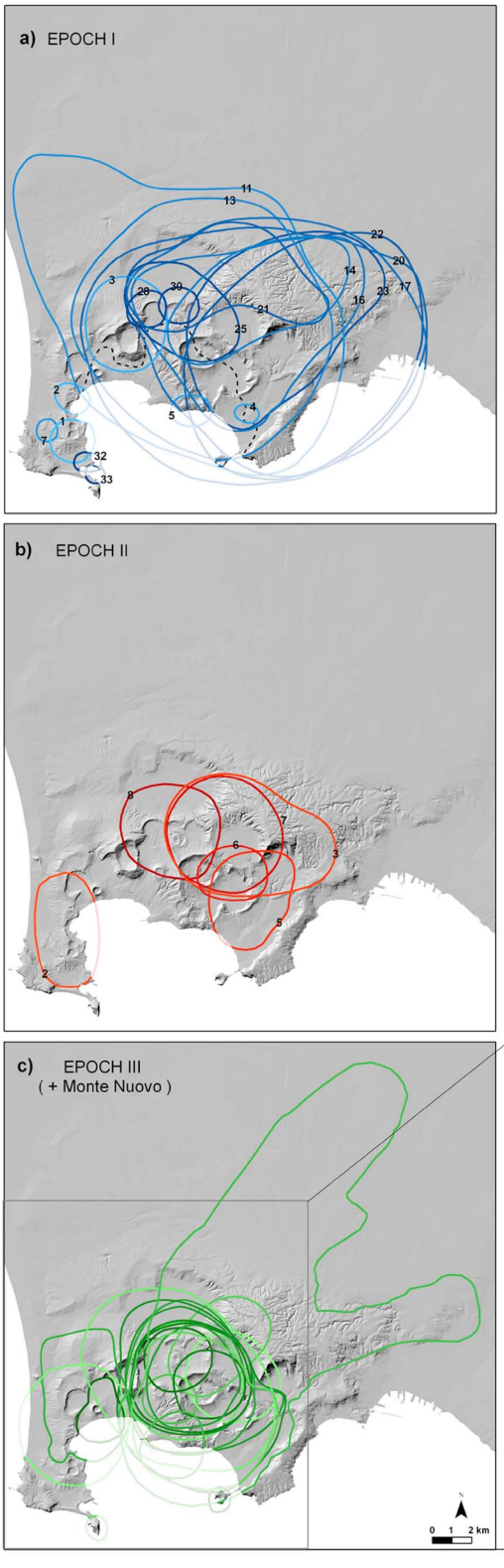

ID	PDC Deposit - Epoch I	Area (km^2)
1	Bellavista Volcano	3.9
2	Mofete Volcano	2.1
3	Gauro Volcano	16.1
4	Santa Teresa Volcano	0.9
5	La Pietra Volcano	2.6
7	Torre Cappella Volcano	1.0
11	Soccavo 1 Tephra	190.5
13	Pomici Principali Tephra	129.2
14	Paleo Pisani 2 Tephra	37.7
16	Soccavo 2 Tephra	75.8
17	Soccavo 3 Tephra	147.5
20	Soccavo 4 Tephra	180.2
21	Paleo San Martino Tephra	37.3
22	Minopoli 2 Tephra	113.6
23	Soccavo 5 Tephra	66.2
25	Pisani 2 Tephra	21.1
28	Montagna Spaccata Tephra	3.0
30	Pisani 3 Tephra	3.0
32	Bacoli Volcano	1.1
33	Porto Miseno Volcano	0.7

ID	PDC Deposit - Epoch II	Area (km^2)
2	Fondi di Baia Tephra	15.7
3	Sartania 1 Tephra	40.7
5	Costa San Domenico Tephra	16.9
6	Pigna San Nicola Tephra	8.0
7	Sartania 2 Tephra	27.0
8	San Martino Tephra	19.7

ID	PDC Deposit - Epoch III	Area (km^2)
2	Agnano 2 Tephra	17.1
3	Averno 1 Tephra	27.0
4	Agnano 3 Tephra	68.0
5	Cigliano Tephra	28.3
7	Capo Miseno Volcano	1.1
8	Monte Sant'Angelo Tephra	43.8
9	Paleoastroni 1 Tephra	18.1
10	Paleoastroni 2 Tephra	5.4
11	Agnano Monte Spina Tephra	312.5
18	Solfatara Tephra	8.7
19	Averno 2 Tephra	24.8
20	Astroni 1 Tephra	39.7
21	Astroni 2 Tephra	19.1
22	Astroni 3 Tephra	41.1
23	Astroni 4 Tephra	60.4
24	Astroni 5 Tephra	29.1
25	Astroni 6 Tephra	26.9
26	Astroni 7 Tephra	10.2
27	Fossa Lupara Tephra	8.9
28	Nisida Tephra	4.7
29	Monte Nuovo Tephra	5.7

Figure 2. Reconstruction of the distribution of PDC deposits generated by explosive events that occurred in (a) Epoch I, (b) Epoch II, and (c) Epoch III plus the Monte Nuovo event. Numbers refer to the events reported in the legend (lines with different color tone indicate different events). Reported deposit boundaries were extended over the sea to allow estimation of reasonable values for PDC invasion area (shown in the legend). Data were derived and updated from *Orsi et al.* [2004]. The distribution shown for the AMS PDCs was derived from *de Vita et al.* [1999]. Naming of events follows *Smith et al.* [2011].

Epoch II, and 20 for Epoch III, in addition to the Monte Nuovo event (i.e., 47 records in total). With respect to the data of *Orsi et al*. [2004], the records of the events of Rione Terra and Archiaverno were deleted from Epoch I, while the records of Capo Miseno and Nisida were moved from Epoch I to Epoch III [*Smith et al*., 2011]. In addition, the reconstruction of the PDC distribution produced for the Agnano Monte Spina (AMS) event by *de Vita et al*. [1999] was considered as an alternative to the data of *Orsi et al*. [2004]. In all cases, part of the PDCs went offshore, so on-land invasion areas were extended over the sea in order to better represent the total area affected by the flow.

The flow area boundaries (Figure 2) refer to the minimum areas invaded due both to the irregular distribution of outcrops and to the large erosive and anthropologic actions affecting the deposits [*Orsi et al*., 2004]. Based on the available field data sets and using alternative expert judgment procedures [*Bevilacqua et al*., 2015], the radial underestimation error of deposit boundaries (treated as epistemic uncertainty) is considered to vary between about 150 and 1000 m, with a mean value of about 500 m [*Bevilacqua et al*., 2015]. It is worth mentioning that such values are comparable with estimates of extended runout shown by surge-like flows with respect to the underlying dense portion of the PDCs, observed in recent eruptions for flows of small-medium scale (see, e.g., *Neri et al*. [2014], for more information). Such an underestimation of the deposit extent could therefore represent a minimum value of the actual flow runout.

In order to use a representative data set of the invasion areas, it was necessary to extend the recorded inundated areas reported in Figure 2 with reasonable estimates for areas of "lost deposits." Based on a comparison between the data sets of invasion areas (Figure 2) and that of the identified vents [*Bevilacqua et al*., 2015, Figures 2 and 3], a number of lost deposits were added to the three epochs. PDC invasion areas up to 10 and 50 km^2 were added as follows: for Epoch I, four records up to 10 km^2 (representing the events of Minopoli 1, Pisani 1, Fondo Riccio, and Concola) and nine records up to 50 km^2 (representing the events of La Pigna 1, La Pigna 2, Gaiola, Paradiso, Paleopisani 1, S4S31, S4S32, Pignatiello 1, and Casale); for Epoch II, one record up to 10 km^2 (representing the event of Baia or a flow from a lost vent); for Epoch III, seven records up to 10 km^2 (representing the events of Agnano 1, Pignatiello 2, Santa Maria delle Grazie, Paleoastroni 3, Olibano Tephra, and two PDCs from lost vents) [*Isaia et al*., 2009; *Smith et al*., 2011]. The choice to add lost deposits of two different areas reflects the fact that the reconstruction of deposits for Epoch I is significantly more difficult than for the later epochs and so larger missing deposits are more likely to be appropriate. The spatial extents invaded by these lost PDCs were sampled using a distribution fitted to available field data sets, truncated with the thresholds mentioned above. This information was treated as another source of epistemic uncertainty besides the radial underestimation.

With the data set of PDC invasion areas defined, it is possible to generate probability density functions of spatial extent distribution considering either the last 5 ka (i.e., Epoch III plus the Monte Nuovo event) or the last 15 ka data sets (i.e., the three Epochs together plus Monte Nuovo). Figures 3a and 3b show the histograms of PDC invasion areas for these two alternative data sets together with the curves of probability density functions derived from them, while Figures 3c and 3d show the corresponding exceedance probability curves (survival functions). In the 5 ka data set, the AMS eruption represents an anomalous value much larger than any other record. In contrast, the presence of several intermediate data points between the body of the empirical distribution for the 15 ka data set and the AMS event allows a quasi-continuous distribution of the PDC inundation areas to be hypothesized and the AMS event to be considered simply one element in a continuous tail distribution, not as an extreme outlier.

The histograms (Figure 3) relate to the inundation areas (Figure 2), while the density and exceedance probability curves include the radial underestimation of PDC inundation areas and the lost deposit areas randomly sampled up to the above defined limits of 10 and 50 km^2 from the distribution of the other invasion area values. The curves, calculated by a Monte Carlo simulation, relate to the 5th, 50th, and 95th percentiles coming from such uncertainty sources and to the maximum likelihood (ML) lognormal distribution, although other distributions were also considered. More details and statistical tests on the adopted distributions are reported in Appendix A. The ML lognormal distribution appears to be the most defendable for characterizing available data sets; from sensitivity analyses, other different but plausible distributions do not significantly change hazard estimate outcomes. Comparison of plots of Figures 3c and 3d indicates that the curves associated with the 5 ka history are very similar to those associated with the 15 ka counterpart, although the latter has a slightly larger number of small events and a slightly fatter tail. We assume these probability

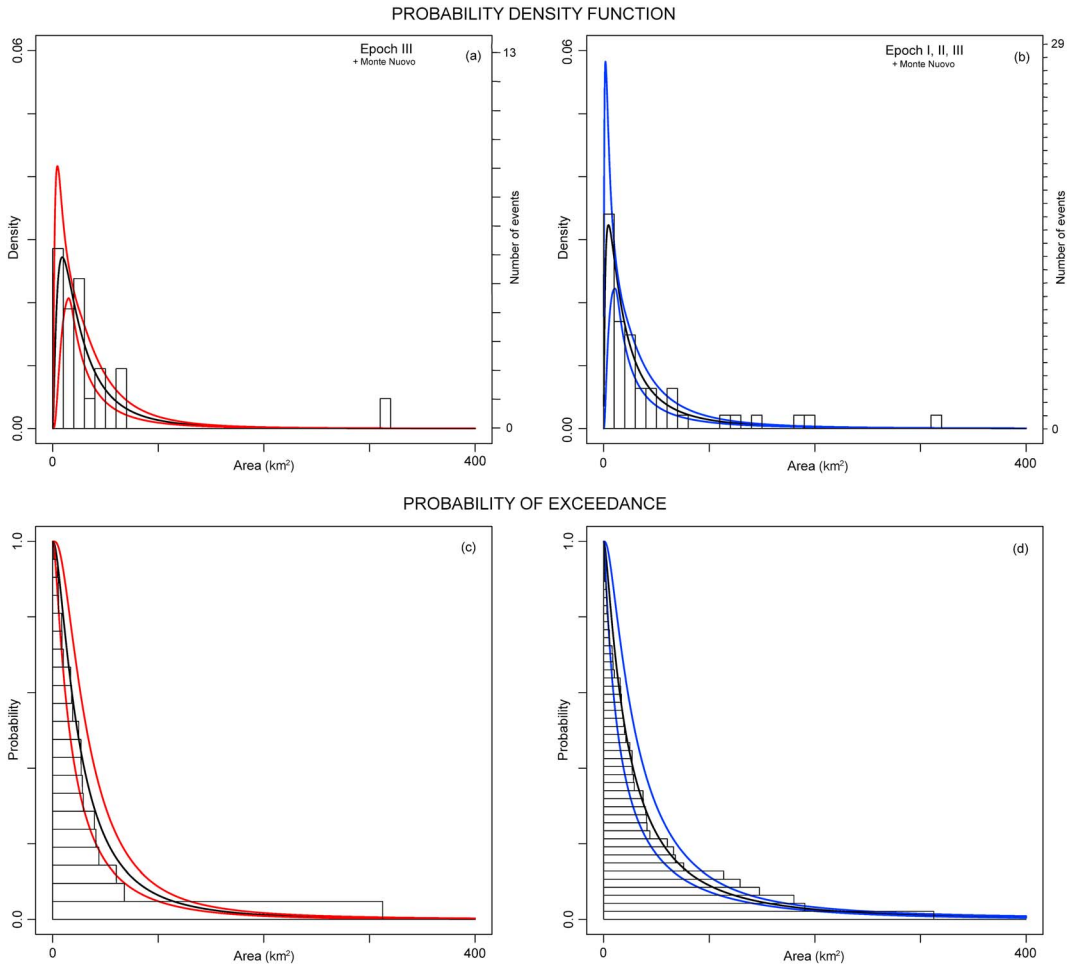

Figure 3. Histograms of the PDC invasion areas as estimated from Figure 2 for (a) Epoch III and (b) all three Epochs (plus the Monte Nuovo event in both cases). Figures 3a and 3b also show probability density functions for the invasion areas after consideration of underestimations of PDC runout and the addition of "lost deposits," as discussed in the text and Appendix A. Figures 3c and 3d show probability exceedance curves (survival functions) corresponding to the two periods considered, 5 ka and 15 ka.

distributions valid over the whole caldera, thus neglecting any dependence of eruptive scale (i.e., PDC invasion area) on vent position or repose time.

2.3. The Simplified PDC Invasion Model

The dynamics of PDCs are particularly complex due to the multiphase nature of the flow, the highly uncertain source conditions, and the complicated interactions of the current with topography [*Druitt*, 1998; *Calder et al*., 1999; *Branney and Kokelaar*, 2002]. At CF volcanoclastic deposits seem to be mostly characterized by surge-like facies, although a quite large variability of transport and emplacement mechanisms can be invoked for different eruptions and even for the same eruptive sequence [e.g., *Valentine*, 1987; *Dellino et al*., 2004]. Some of these complexities can be investigated by 2-D/3-D numerical simulations of the partial collapse of the eruption column and propagation of PDCs over topography [e.g., *Todesco et al*., 2006; *Esposti Ongaro et al*., 2008b]. Such simulations explored, for instance, the influences of different collapsing regimes in the column and of vent positions on the PDC features. However, due to the large computation time needed to produce such simulations (of the order of some days with parallel computing), it is impractical and expensive to apply this kind of modeling within Monte Carlo algorithms involving thousands of simulations.

Therefore, with the aim of exploring main effects of the large variability of vent location and eruptive scale (i.e., PDC invasion area) on the area inundated, a simple integral PDC propagation model is adopted here.

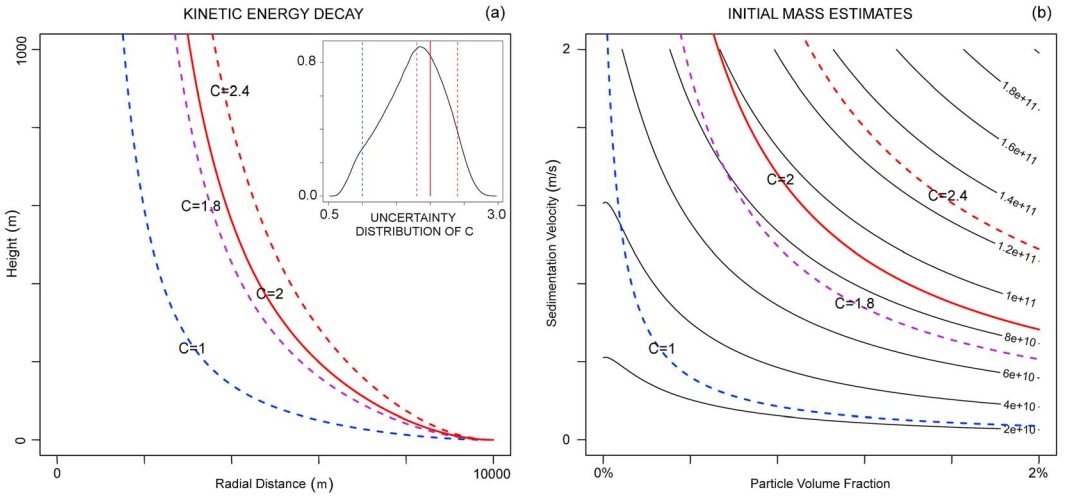

Figure 4. (a) Example of decay of radial flow head kinetic energy expressed in terms of potential height as a function of distance from the source. Curves refer to a flow runout of 10 km and to values of the *C* parameter equal to 1.0, 1.8, 2.0, and 2.4 ($m^{2/3}/s$), as reported in the labels. In the inset the probability distribution of the *C* parameter is shown once a uniform distribution is assumed on the physical variables forming it (see Appendix B for more details). (b) Estimates of the initial mass of pyroclastic material of the column collapsing to the ground as a function of the initial concentration of pyroclasts and their sedimentation velocity (see Appendix B). All curves refer again to a radial flow runout of 10 km, whereas the colored lines refer to the four values of the *C* parameter reported in Figure 4a.

The model is based on the so called *box model* of *Huppert and Simpson* [1980], *Dade and Huppert* [1996], and *Hallworth et al*. [1998] and is suited to describing the propagation of turbulent, particle-laden currents, in which inertial effects dominate over viscous forces and particle-particle interactions. The model has been validated and calibrated through extensive comparison with 2-D numerical simulations produced with the PDAC model [*Neri et al*., 2003; *Esposti Ongaro et al*., 2007, 2011]. A brief description of the model and its comparison with 2-D numerical simulations is reported in Appendix B.

The integral model allows computation of flow kinematics and the maximum distance (flow runout) reached over a subhorizontal surface by a current generated by instantaneous release (i.e., dam break configuration) of a finite volume of gas and solid particles, at a given concentration. Based on outcomes of numerical simulations [e.g., *Todesco et al*., 2006; *Esposti Ongaro et al*., 2008b], such a generation mechanism describes reasonably well the unsteady release of a portion of the column collapsing to the ground. The box model assumes that the current is vertically homogeneous and deposits particles during propagation as a function of their (constant) sedimentation velocity. No effect of wind or other atmospheric conditions is considered by the model. In the present application the model is used in its simpler formulation, which assumes a single particle size representative of the mean Sauter diameter of the grain-size distribution of the mixture. The integral model can therefore compute the flow front velocity, the average flow thickness, and the particle concentration as a function of time, assuming either axisymmetric or unidirectional propagation, from which the kinetic energy (or dynamic pressure) of the flow front can be calculated.

In order to quantify main effects of topography on the propagation of a PDC, the flow kinetic energy is compared to the potential energy associated with, and therefore required to overcome, the topographical relief that the flow encounters, thus following the same approach of the energy line (or energy cone) model [*Hsu*, 1975; *Alberico et al*., 2011]. It is worth noting, however, that the integral model allows a more realistic description of the propagation of a turbulent flow compared to the energy line, which instead assumes a simple linear decay of flow kinetic energy more appropriate for describing the dynamics of landslides and high-concentration granular flows (not commonly outcropping at CF). For instance, Figure 4a illustrates the nonlinear decay of the flow kinetic energy, expressed as potential height for a radial flow with runout 10 km, as a function of distance from source and as a function of the *C* parameter ($m^{2/3}/s$) which accounts for the initial volume concentration of particles and their sedimentation velocity in the flow (see Appendix B for more details).

In order to rely on the data set of PDC invasion areas described in the previous subsection, in this study the PDC invasion model is applied in an inverse mode, i.e., starting from the invasion area (obtained using the density functions described above) and then computing the volume (or the equivalent pyroclast mass) required to generate such propagation, given a specific vent location and surrounding topography. Figure 4b shows the mass of pyroclasts collapsing to the ground that is able to generate a radial PDC with runout 10 km, as a function of the initial pyroclast volume concentration and sedimentation velocity, considering a flat topography. The physical parameters of the flow adopted in the integral model are assumed representative of the eruptive mixture and collapse conditions at CF [e.g., *Dellino et al*., 2004; *Todesco et al*., 2006; *Esposti Ongaro et al*., 2008a, 2008b]. More details on the numerical procedure and the parameters we use are provided in Appendix B.

3. Results

Combining the spatial probability map of new vent opening, the probability distribution of PDC invasion areas, and the PDC integral box model described above, it is possible to produce several probabilistic hazard maps of PDC invasion with their associated uncertainty. In the following, a few cases are shown and discussed to illustrate our main findings. Several other maps were produced to investigate the influence of some key variables or assumptions on the hazard mapping. Our maps relate solely to the probability of invasion by PDCs and not to the distributions of specific hazard variables, such as dynamic pressure and temperature. We also assumed that a future PDC episode will originate in the on-land portion of the caldera because source conditions would be fundamentally and significantly different in the case of an underwater vent.

Our invasion maps are the result of a Monte Carlo simulation procedure, implemented to combine the several probability distributions discussed above (aleatoric variabilities) together with their epistemic uncertainties, based on a doubly stochastic model. The Monte Carlo simulation has a nested structure, configured for estimating uncertainty on the results: as a consequence, the procedure creates maps of PDC invasion in terms of a mean (or median) value and of representative percentiles with respect to the uncertainty sources we consider. With the location of the eruptive vent determined and the value of the area to be invaded by the flow defined, the simulation of a single PDC propagation event associates a value of 1 to those zones reached by the flow, and 0 otherwise. This is done using the PDC flow model in inverse mode and including the blocking effect of the topography (Appendix B). Therefore, for each outcome of the epistemic uncertainty sources (i.e., uncertainty on the probability map of new vent opening and uncertainty on the density distribution of the PDC invasion area), by repeating the simulation of a single PDC, a large number of times randomly changing vent location and inundation area, and then aggregating the zone 0/1 values obtained to estimate their means, it is possible to approximate, by the law of large numbers, the probability that each location of the map is reached by a PDC conditional on the occurrence of an explosive eruption. To limit computation time, most of the maps are produced using a regular Cartesian grid of cells with 500 m sides, although simulations were also performed with higher resolutions to investigate the sensitivity of results to this numerical parameter. For instance, a grid of cells with 250 m sides produced maps similar to those using 500 m resolution. Based on the 500 m grid and due to the nested structure of the Monte Carlo procedure, each invasion map requires the execution of over half million model simulations.

Figure 5 shows the PDC invasion probabilities in terms of a mean map and maps of the 5th and 95th percentiles, assuming the vent opening probability maps of Figure 1 and the probability distribution of invasion areas associated with the 5 ka data set (see Figures 3a and 3c). The PDC invasion probability maps assume that each new event would be able to produce PDCs just from a single vent located in the on-land portion of the caldera. With reference to the mean map, from the distribution of isolines of equal invasion probability it emerges that, consistent with the deposit data [e.g., *Orsi et al*., 2004], the central eastern part of the caldera is the most exposed to PDC hazard with peaks of probability of invasion of about 53% in the Agnano plain. Probabilities above 45% are also computed in the Astroni area and above 30% in the area of Solfatara. Note that mean probability values above 5% apply to almost all parts of the caldera (with the exception of a small portion of the Capo Miseno peninsula), and a large part is associated with mean values exceeding 10% PDC invasion probability. Values between about 5 and 10% affect some areas outside the caldera border (e.g., Collina di Posillipo and some neighborhoods of Naples). The plots showing 5th and

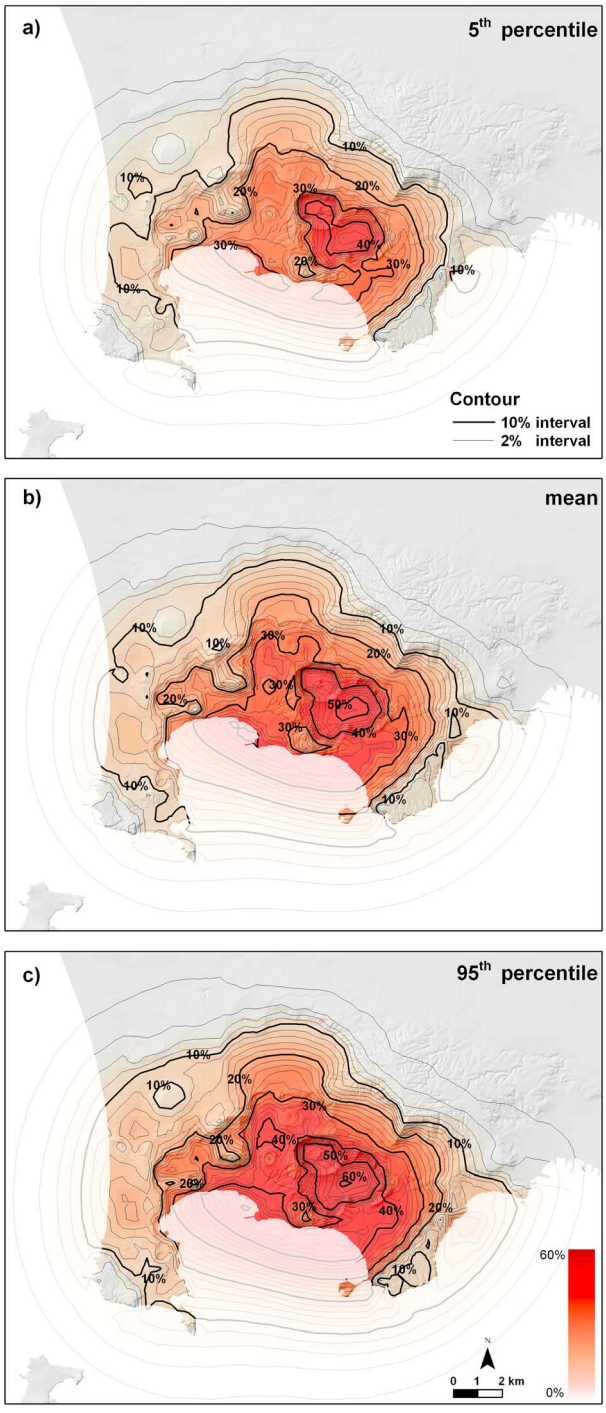

Figure 5. PDC invasion probability maps computed by assuming the vent opening distribution described in Figure 1 and the spatial density distribution of invasion areas of the last 5 ka, shown in Figure 3a. The maps assume that PDCs originate from a single vent per eruption and that the vent is located in the on-land part of the caldera. Contours and colors indicate the percentage probability of PDC invasion conditional on the occurrence of an explosive eruption. The maps relate to (a) the 5th percentile, (b) the mean spatial probability, and (c) the 95th percentile, respectively.

95th percentiles (Figures 5a and 5c) enumerate the substantial uncertainty on these mapped probabilities of PDC invasion with respect to the sources of epistemic uncertainty described above. These maps apply only to the propagation of PDCs over the landward portion of the caldera; isolines of the probability of invasion in offshore parts of the caldera are shown in outline to give a first approximation of the potential hazard represented by PDCs traveling over the sea. We assume the sea surface as flat ground topography with no effect of the water on the PDC propagation (thus neglecting any specific heat and mass transfers between flow and sea), although theoretical studies have pointed to a reduced mobility of PDCs over water [e.g., *Dufek and Bergantz*, 2007]. The data of the three maps shown in Figure 5 are reported in the Data Sets S1, S2, and S3, respectively, in the supporting information.

Figure 6 shows the same maps as Figure 5 but in this case assumes the probability distribution of invasion areas derived from events over the last 15 ka (see Figures 3b and 3d). The maps are very similar to those of Figure 5, with a slight increase in areas affected by low probabilities of invasion (see, for instance, the 2–10% isolines) and an associated slight decrease of the peak values computed in the central eastern part of the caldera. As mentioned above, these effects are the result of the slightly fatter tail of the distribution related to the 15 ka history compared to that of the 5 ka record (see Figure 3).

Several other maps, for the sake of brevity not described here, were also produced, some of which are reported in Figure 7. These investigate the effects on the PDC invasion probability maps of (i) the procedure followed for the definition of the vent opening map (i.e., kernel function versus partitioning of the caldera, see *Bevilacqua et al.* [2015], for explanations) (Figure 7b); (ii) neglecting fault, fracture, and homogeneous distribution maps in the definition of the vent opening map (see again *Bevilacqua et al.* [2015] (Figure 7c); (iii) considering only the vent locations of Epoch III in the definition of the vent opening probability map (Figure 7d);

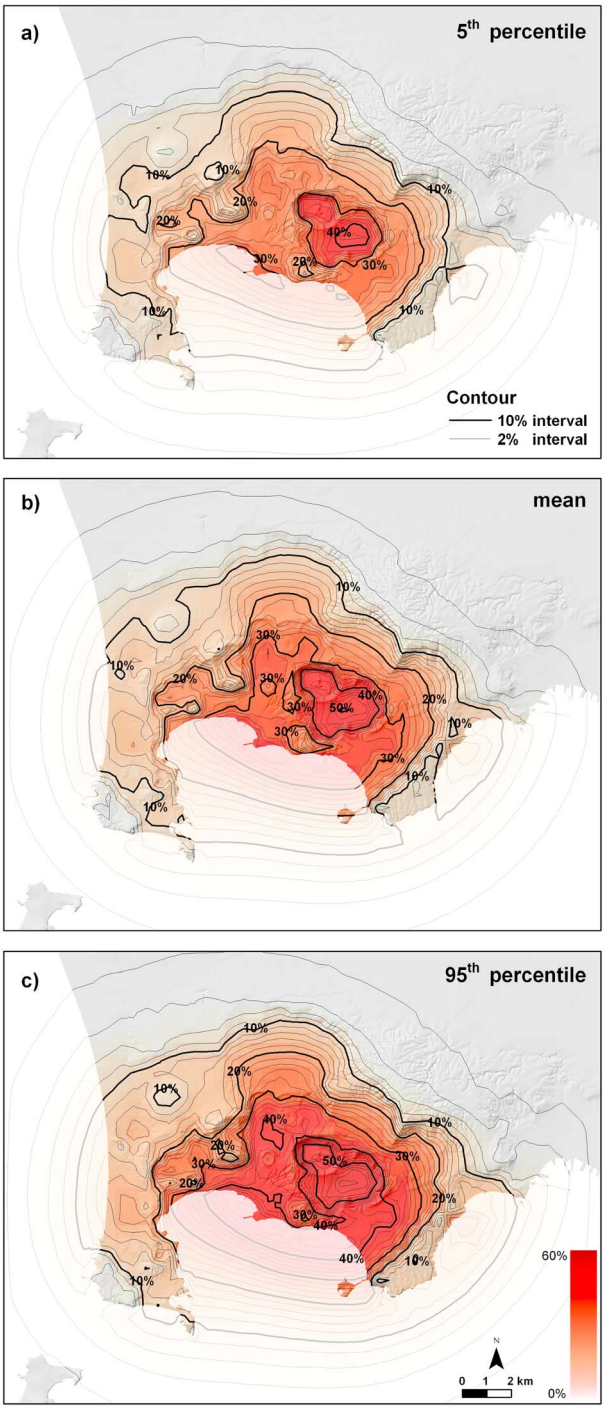

Figure 6. PDC invasion probability maps computed by assuming the vent opening distribution described in Figure 1 and the spatial density distribution of invasion areas of the last 15 ka, shown in Figure 3b. The maps assume that PDCs originate from a single vent per eruption and that the vent is located in the on-land part of the caldera. Contours and colors indicate the percentage probability of PDC invasion conditional on the occurrence of an explosive eruption. The maps relate to (a) the 5th percentile (b) the mean spatial probability, and (c) the 95th percentile. Note that the color scale used in these maps is consistent with that used in Figure 5.

(iv) different physical properties of the flows adopted in the PDC invasion model (Figure 7e), and (v) the vent opening probability map of *Selva et al*. [2012] (Figure 7e). Some more details on the specific parameters used to produce these maps are given in the caption to the figure. As it emerges from the comparisons, despite some significant differences observed locally in specific areas of the caldera, our main findings about the spatial distribution of PDC invasion probabilities remain largely valid.

Our method also enables us to draw probabilistic invasion maps that consider eruption events constrained below a defined upper scale limit (in our analysis, up to a defined PDC invasion area). This can be obtained straightforwardly by truncating the eruptive scale distributions of Figures 3c and 3d at a given limit. For instance, Figure 8 shows PDC invasion maps representative of the mean, and 5th and 95th percentiles of the distribution, when the limiting value corresponds to 5% exceedance probability of the PDC invasion areas with reference to the 5 ka curve (Figure 3c). Based on the estimates of the probability of occurrence at different eruptive scales, as computed by *Orsi et al*. [2009], such a limit approximately corresponds to the occurrence of explosive eruptions of small and medium scale but not large-scale events (e.g., the AMS eruption; the average probability of occurrence of large eruptions is, in fact, estimated to be about only 4% of all scale sizes). Under this restriction, the resulting PDC invasion maps (Figure 8) remain similar to those that consider the full distribution of eruptive scales (Figures 5 and 6). However, in Figure 8 the probability isolines now affect slightly smaller areas due to the neglecting of PDCs produced by large-scale events. Of course, maps of the same type could be produced for other thresholds associated with other probabilities of exceedance of the PDC invasion areas (Figures 3c and 3d).

Finally, we investigate the possibility of simultaneous or near-simultaneous openings of multiple vents in zones of the caldera significantly distant to each other

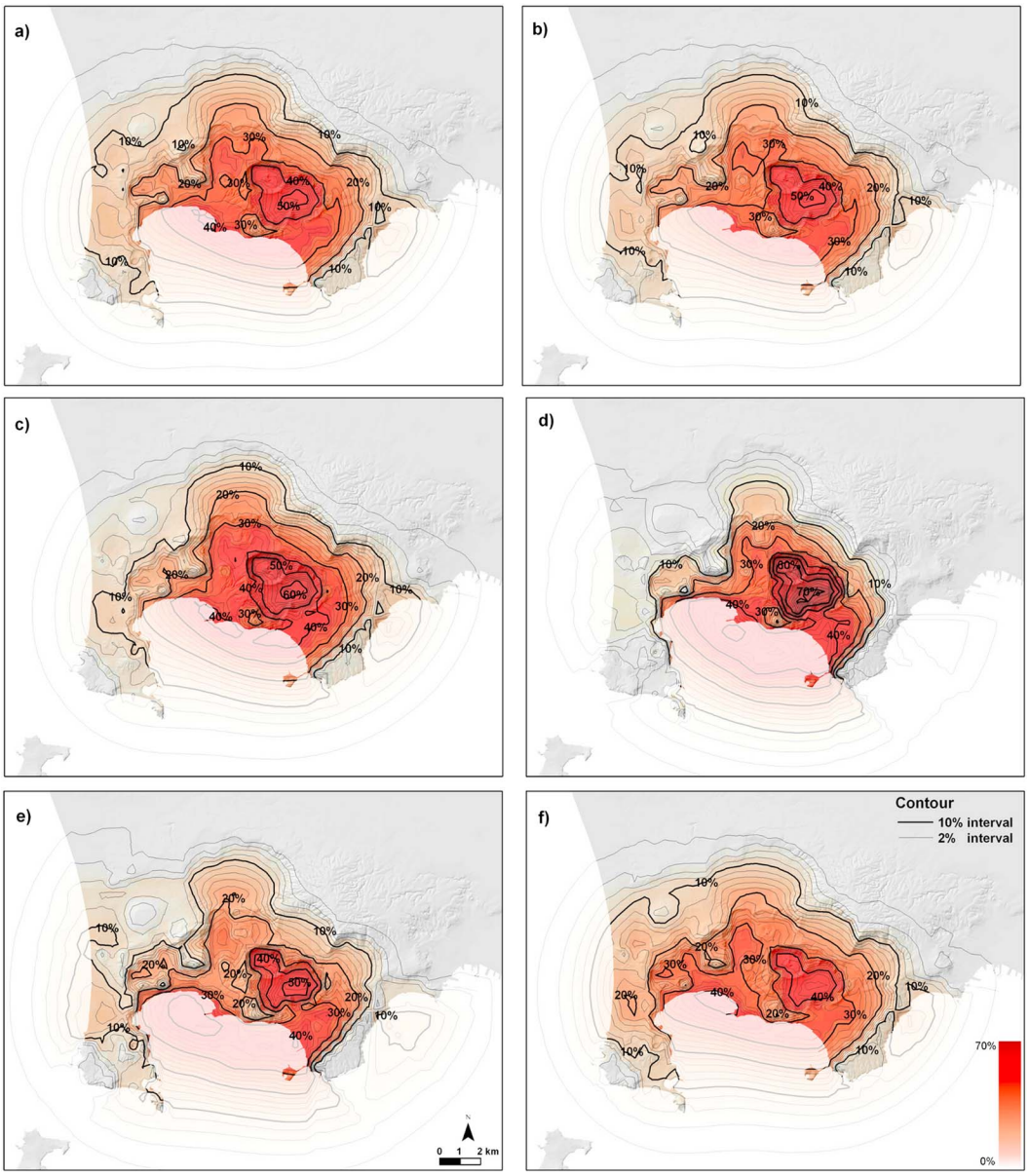

Figure 7. Ensemble of mean spatial probability maps of PDC invasion showing the effect of different assumptions on the hazard mapping. (a) Reference mean map assuming the vent opening map of Figure 1 and the spatial density distribution of PDC invasion areas of the last 5 ka (as in Figure 5b of this paper); (b) PDC invasion mean probability map assuming the vent opening probability maps of Figures 8a–8c of *Bevilacqua et al.* [2015], based on the use of kernel functions (see *Bevilacqua et al.* [2015], for more details); (c) mean map obtained by neglecting the influence of fault, fracture, and homogeneous distribution maps on vent opening probability [see *Bevilacqua et al.*, 2015]; (d) mean map obtained considering only the distribution of vent location of the events of Epoch III; (e) mean map obtained by assuming a value of the *C* parameter equal to 1 $m^{2/3}/s$ instead of 2 $m^{2/3}/s$, as assumed in all other maps (see Appendix B for more details), and (f) mean map obtained by assuming the vent opening map of *Selva et al.* [2012]. Contours and colors indicate the percentage probability of PDC invasion conditional on the occurrence of an explosive eruption. Note that the color scale used in these maps is consistent with those used in Figures 5 and 6. See text for more explanation.

(i.e., not related to vent migration within the same area). Such occurrences are indeed a possible scenario at a caldera, as shown at Rabaul volcano (Papua New Guinea) in September 1994, with the simultaneous opening of the vents of Tavurvur and Vulcan volcanoes, on opposite sides of the caldera (8 km distant from each other) [*Roggensack et al.*, 1996]. Recent work [*Isaia et al.*, 2009] has shown that such a phenomenon likely occurred also at CF with the contemporaneous eruption, about 4.3 ka B.P., of the Solfatara and Averno centers, located

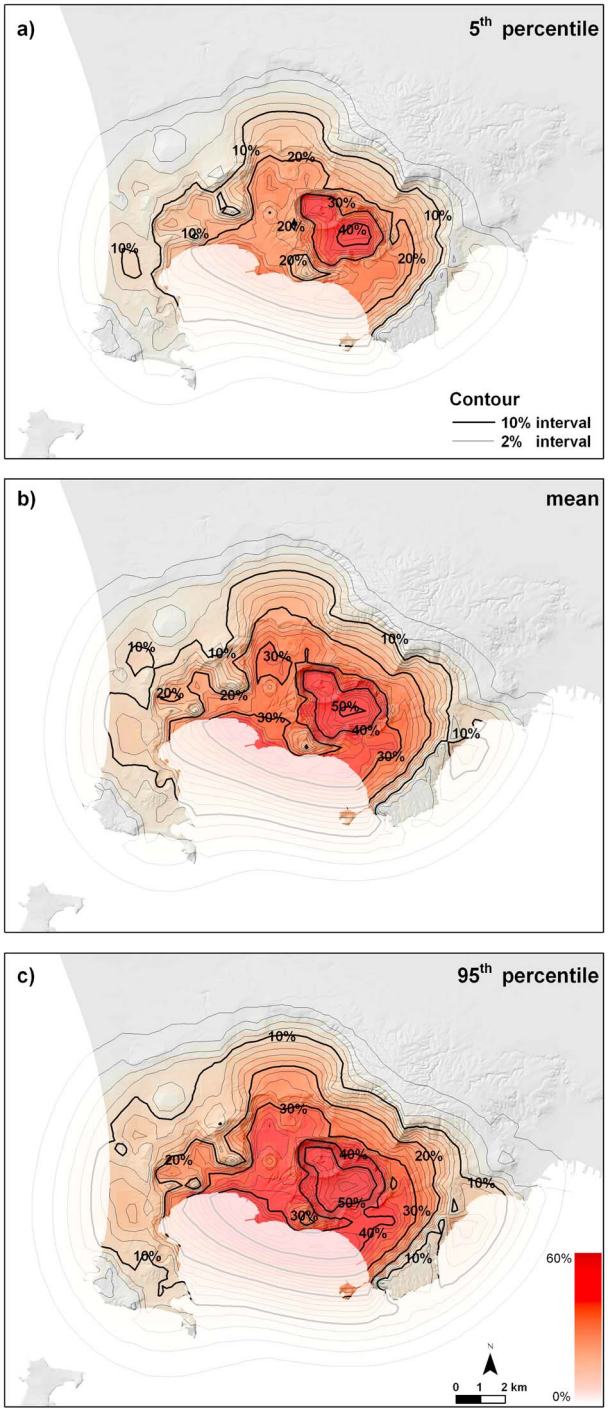

Figure 8. PDC invasion probability maps computed by assuming the vent opening distribution described in Figure 1 and the spatial density distribution of invasion areas of the last 5 ka shown in Figure 3a with a bounding limit corresponding to 5% exceedance probability for invasion area. The maps assume that PDCs originate from a single vent per eruption and that the vent is located in the on-land part of the caldera. Contours and colors indicate the percentage probability of PDC invasion conditional on the occurrence of an explosive eruption. The maps relate to (a) the 5th percentile, (b) the mean spatial probability, and (c) the 95th percentile. Note that the color scale used in these maps is consistent with those used in Figures 5–7.

about 5.4 km apart (i.e., the events of Solfatara and Averno2, *Bevilacqua et al.* [2015]. Tephra placed at the same height of the CF stratigraphic record [e.g., *Di Vito et al.*, 1999; *Smith et al.*, 2011] and still not chemically and physically correlated suggest that other groups of eruptions could have been simultaneous. Multiple venting implies therefore the possibility of an increased area potentially invaded by PDCs in an eruptive episode, both inside and outside the caldera.

Based on all the available evidences at CF and elsewhere, the probability of the opening of two simultaneous vents is estimated from expert judgment to be about 10%, but with an uncertainty range from about 5% to 25% (corresponding to the 5th and 95th credible range percentiles, see *Bevilacqua et al.* [2015], for details). Based on these numbers, Figure 9 shows PDC invasion probability maps for the scenario of two simultaneous vents in terms of (a) the 5th percentile, (b) the mean map, and (c) the 95th percentile. No constraint was imposed on the distance between the two simultaneous vents. Based on the probability map of vent opening, a mean distance between dual vents of 4.7 km was calculated (assuming two independent samples from the same spatial distribution), with 5th and 95th percentiles of 1.0 and 10.0 km, respectively.

The maps of Figure 9 are comparable to those of Figure 5 in the sense that they assume, for both eruptive centers, the same probability of vent opening of Figure 1 and the probability density function of the PDC invasion area of the last 5 ka. In this scenario, the area invaded by the flows generated by two simultaneous vents is computed as the union of the areas invaded by the PDCs that originate from the two distinct vents. From comparison with the maps of Figure 5, it emerges that in the scenario with dual venting the peak probabilities computed in the Agnano plain are about 5% higher and also that the isolines representative of the 5% and 10% probability of invasion occupy, in this situation, slightly wider areas.

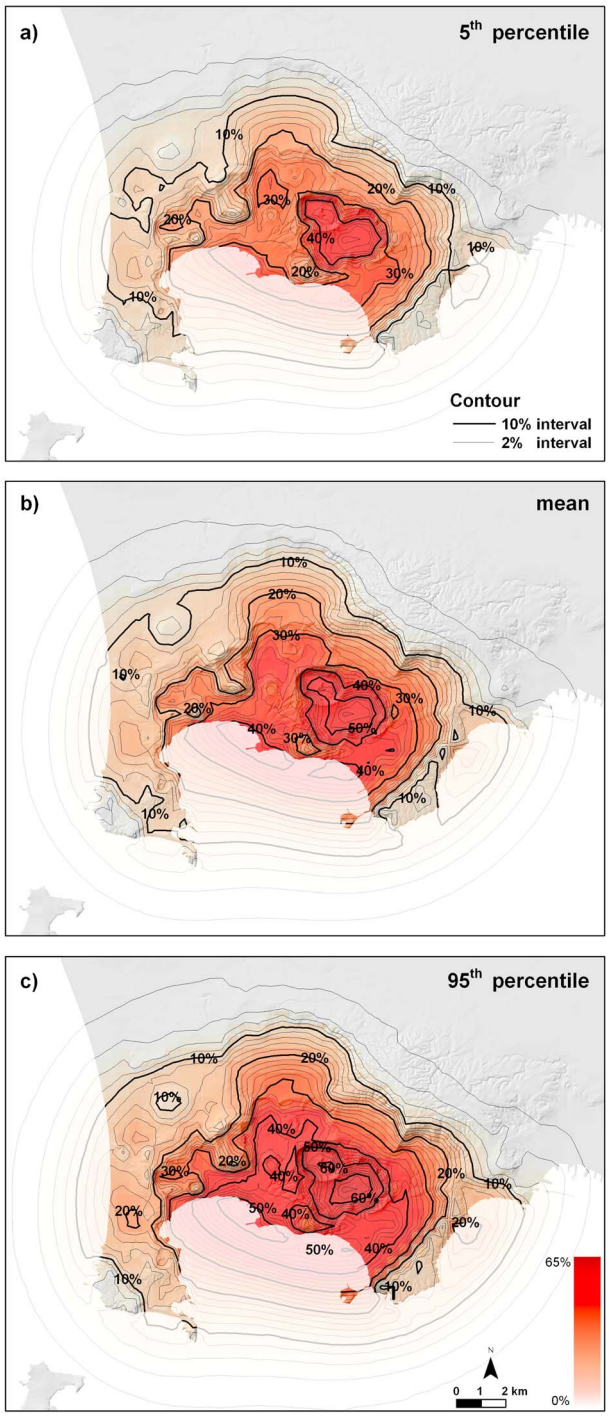

Figure 9. PDC invasion probability maps computed for PDCs that originate from two simultaneous vents in an eruptive event, with the vents located in the on-land part of the caldera. The calculations assume the vent opening distribution described in Figure 1 and the spatial density distribution of invasion areas of the last 5 ka, shown in Figure 3a. Contours and colors indicate the percentage probability of PDC invasion conditional on the occurrence of an explosive eruption. The maps relate to (a) the 5th percentile, (b) the mean spatial probability, and (c) the 95th percentile. Note that the color scale used in these maps is consistent with those used in Figures 5–8.

4. Discussion

In this study, we develop an innovative method to generate probabilistic maps of PDC invasion in caldera settings conditional on the occurrence of an explosive eruption. Our approach allows different strands of data to be combined within a probabilistic framework and, most importantly, enables us to consider and quantify the influence of some key sources of epistemic uncertainty present in the volcanic system. The approach is particularly relevant for caldera settings due to the large variations of possible vent locations and eruption scales that can be exhibited by volcanoes of this type (aleatoric variabilities).

In the present case of CF, PDC invasion maps are obtained by conflating a probabilistic distribution for new vent opening position [*Bevilacqua et al.*, 2015], a distribution of PDC invasion areas assumed representative of the range of eruption scales (based on an updated version of the data set of *Orsi et al.* [2004]), and a simplified PDC invasion flow model able to account for the PDC scaling properties and the main effect of caldera topography on the extent of areas invaded by the flows. These probabilistic distributions are also able to account for some of the main epistemic uncertainties affecting the volcanic system [see *Bevilacqua et al.*, 2015]. In particular, the analysis takes account of the uncertain location of past vents; the number of "lost vents"; the uncertain correlations between the distribution of observable features of the caldera, such as faults and fractures, and the spatial probability of vent opening; the incomplete reconstruction of areas invaded by previous PDCs, and the possibility to have simultaneous activation of two distinct vents during the same eruptive episode. Our analysis relies on evidence about the last 15 ka of activity of the volcano and therefore does not include extreme caldera-forming events such as the CI or the NYT eruptions. Moreover, all the maps presented here presume that the eruptive vent openings take place in the landward portion of the caldera; offshore eruptions are, fundamentally, a different and more difficult problem to tackle.

We provide PDC invasion maps under different assumptions in order to investigate their relative relevance and the robustness of the results. Assuming the activation of a single vent per eruptive event, it emerges from these maps that the whole caldera is significantly exposed to PDC hazard (e.g., Figure 5). Mean invasion probabilities above 5% are calculated over almost the whole caldera, with peak values just exceeding 50% in the Agnano plain. The areas of Astroni and Solfatara are exposed with mean values above about 30%. Mean probabilities of about 10% are also computed in some areas outside the caldera, in particular, over Collina di Posillipo and in some neighborhoods of the city of Naples. Consideration of the density distribution of PDC invasion areas over the last 15 ka (see Figure 6) does not affect significantly the probability distribution described above but just slightly extends the area affected by low-probability isolines, simultaneously slightly reducing peak value probabilities in the central eastern part of the caldera. Different assumptions about the vent opening mapping and PDC properties also produce changes to the probability values of about the same amount, as shown in the additional maps reported in Figure 7.

These maps also allow the influence of different eruption scenarios to be considered. Figure 8, for instance, relates to the possibility to define an upper limit on the expected eruptive scale of a future event. Specifically, the probability distribution of the PDC invasion areas (Figure 3) was restricted to its 95th percent value to produce Figure 8. This limit represents approximately the occurrence of small to medium scale events at CF, but not large-scale events (such as the AMS event) [*Orsi et al*., 2009]. Under this constraint, the computed distribution of probability results is again very similar to that described above but in this case with a general decrease in mean values of about 2%. Nevertheless, essentially the whole caldera is still characterized by mean probabilities of flow invasion larger than 5%, and values up to about 10% are again computed in some eastern areas outside the caldera rim.

Similarly, Figure 9 considers the possibility of simultaneous activation of two separate vents during the same eruptive event. This possibility has been postulated as having happened already at CF [*Isaia et al*., 2009] and has the effect of increasing the area potentially affected by PDC invasion. Assuming that this scenario could occur in 10% of all eruption episodes, with a credible range between about 5% and 25%, the resulting mean invasion map produces slightly wider inundation footprints with a general increase of probability values of about +2% compared to the case of single vent.

An important outcome of our approach is the possibility to identify and quantify some of the sources of epistemic uncertainty affecting the phenomena of concern. This permits us to generate not only a mean (or expected value) map of the probability of PDC invasion but also a set of maps that represent 5th and 95th percentile uncertainty spreads. From inspection of the results, the difference in relative percentage between the 5th or 95th percentiles and the local mean values (i.e., divided by such mean values) can be approximately quantified inside the caldera typically as ±25% of the mean probability values, with variability from about ±15% up to ±35% (corresponding to the 5th and 95th percentiles) in different areas of the caldera. Outside the caldera the average variability rises to about ±55% of the local mean, with ranges from about ±30% to ±110% from place to place. Despite the significant sizes of such uncertainty estimates, in the present analysis just some of the relevant sources of epistemic uncertainty were considered, as previously described. Other possible influences, for instance, dependence of vent location and temporal patterns on eruptive scale, the effect of eruption duration, the accuracy of the PDC propagation model, complexities of 3-D topography on flow propagation, as well as the potential influence of atmospheric conditions, are not included in the present analysis and could represent objectives of future studies.

The limitations of the PDC propagation model and of the stopping criterion should be considered when evaluating the invasion maps. The integral box model does not take into account complex processes occurring during PDC propagation, such as partial blocking of the current by topographical barriers, the generation of buoyant thermals and coignimbrite columns from disruption of the main flow or by passing over topographic obstacles, and the complex multidimensional and transient effects associated to the interaction of a flow with the ground topography [*Todesco et al*., 2006; *Esposti Ongaro et al*., 2008b]. The effect of wind on the propagation of the PDCs is also neglected. Moreover, our maps are computed on a Cartesian grid with cells of side measuring 500 m, meaning that the associated probability should be interpreted as a mean value over the cell space and that details below this scale are not meaningful. This is the case, for instance, for some small island-shaped probability contour areas located mostly over Collina di Posillipo and eastward that are generated by the complex interplay between the envelope of all simulations with

varying vent location and scale and the rough topography of the caldera. As a consequence, detailed local-scale zonation of the flow invasion probabilities cannot be achieved using the approach illustrated here. For that purpose, more accurate transient and multidimensional physical models and more detailed analyses of local topography should be used.

The probabilities of flow invasion reported in all the maps (Figures 5–9) are conditional, as mentioned above, on the occurrence of an explosive eruption from a vent or vents in the subaerial portion of the caldera. This means that to compute the probability of invasion conditional on the occurrence of an unspecified eruption (i.e., effusive or explosive, with vents located on land or offshore), it is necessary to multiply all the probability isoline values by $(1 - P)$, where P is the probability of being effusive (assuming, for the sake of simplicity, an equal vent opening spatial distribution for explosive and effusive eruptions) or the probability of having a vent located in the sea (hence not producing a significant PDC hazard in the common sense). By assuming a probability of occurrence of an effusive eruption of about 10% [see *Orsi et al*., 2009] and a probability of occurrence of an eruption with vent located offshore of about 25% [see *Bevilacqua et al.,* 2015], the probability values reported on the maps presented here need to be multiplied by a factor $(1 - P)$ of about 0.68 (assuming the two circumstances to be independent).

Finally, it is possible to highlight the notable probability that a CF PDC originating on land would likely interact with seawater. Significantly wide areas along the coast of the municipality of Pozzuoli have associated mean probabilities of flow invasion up to about 40%, with all the coast of the Golfo di Pozzuoli being potentially affected with mean probabilities above 10%. The generation of a PDC-induced tsunami should therefore be considered a possibility, such as that observed during the 1994 eruption of Rabaul [*Nishimura et al*., 2005] and the eruptive crises of the Soufrière Hills volcano, Montserrat [*Mattioli et al*., 2007]. This adds the hazards associated with PDC-induced tsunami waves to those of other hazardous processes generated by potential explosive events with a vent located offshore, which possibility is estimated to have a mean probability of occurrence of about 25% (based on *Bevilacqua et al.* [2015]).

5. Conclusions

PDCs represent one of the most dangerous volcanic hazards for people living in proximity to explosive volcanoes. The hazard zonation of areas potentially affected by this threat is therefore of paramount importance and is the first step needed to draw up appropriate mitigation measures. The CF caldera represents a prime example of this type of high-risk volcano. Despite the fact that CF has been the object of many studies in recent decades, the mapping of PDC hazard there remains particularly challenging due to the remarkable variability of potential vent locations and eruption scales, and the complex dynamics of PDC movement over the caldera topography.

Here we have produced, through the application of a doubly stochastic model, the first quantitative background (or long-term/base-rate, i.e., in conditions of no unrest) probabilistic maps of PDC invasion able to incorporate some of the main sources of epistemic uncertainty that influence the models for aleatoric (physical) variability. In particular, the new method developed combines the spatial probability distribution of vent opening locations [*Bevilacqua et al*., 2015], the density distribution of PDC invasion areas, and a simplified PDC model able to describe the main effect of topography on flow propagation.

Our results clearly suggest that the entire caldera has potential to be affected, with a mean probability of flow invasion higher than about 5% and the central eastern area of the caldera (i.e., Agnano-Astroni-Solfatara) having invasion probabilities above about 30% (with local peaks at or above 50% in Agnano). Significant mean probabilities (up to values of about 10%) are also computed in some areas outside the caldera border (i.e., over Collina di Posillipo and in some neighborhoods of Naples). Our findings are robust against different assumptions about several of the main physical and numerical parameters adopted in the study.

In addition to mean values of probability of PDC invasion, this study provides the first estimates of the credible uncertainty ranges associated with such probability estimates in relation to some key sources of epistemic uncertainty. From our analysis, uncertainty spreads on invasion probabilities inside the caldera typically range between ±15 and ±35% of the local mean value, with an average of about ±25%; wider

uncertainties are found outside the caldera, with an average above ±50% and a significantly larger range of variability from place to place. Despite the several assumptions and limitations of this study, including the subjectivity of the approach followed, such first estimates of epistemic uncertainty provide crucial information that needs to be carefully accounted for when quantifying the likelihood of PDC hazards and risks associated with a future eruption occurring in the CF.

Appendix A: Class of Distributions Representing the PDC Invasion Areas

In order to choose which distribution fits the data sets reported in Figure 3 better, i.e., the 5 ka data set (D1, Figures 3a and 3c) or the 15 ka data set (D2, Figures 3b and 3d), we performed some analyses and statistical tests. In particular, we focused on the maximum likelihood (ML) lognormal, the ML Weibull, and the Pareto distributions.

Recall that the density function of a lognormal distribution of log mean m and log standard deviation s, is

$$f_{LN}(x) = \frac{1}{x\sqrt{2\pi s^2}} \exp\left(-\frac{\log^2(x-m)}{2s^2}\right) = \frac{s\sqrt{2}}{x\sqrt{\pi}}(x-m)^{-\log(x-m)}.$$

whereas the density function of a Weibull distribution of mean $\lambda > 0$ and shape $k > 0$ is

$$f_W(x) = \frac{k}{\lambda^k} x^{k-1} \exp\left(-(x/\lambda)^k\right).$$

In the first case, the logarithm and the exponential terms of the expression counterbalance each other to a certain extent and produce a quasi-polynomial decay although faster in the limit. In the second case, the distribution produces a quasi-exponential tail although slower in the limit. While both distributions fit quite well the body of the data sets, the lognormal distribution gives higher likelihood to the largest values. Statistical analyses were performed in order to quantitatively evaluate the effect of this choice.

Some criteria were unable to discriminate between the two distributions. The Akaike information criterion values (i.e., the logarithm of the maximal likelihood) are very similar for both data sets and therefore could not provide useful indication as to preference. Similarly, a measure of fitting error was unable to give a clear difference between the two distributions. We define the fitting error E as the L^1 distance between the cumulative function of our estimation choice and the cumulative empirical function of the observed data, rescaled in proportion to the range of the data set. In the case of data set D1, the fitting errors of the ML lognormal and ML Weibull resulted in values about 4.8×10^{-2} and 5.5×10^{-2} respectively; conversely for the data set D2, values of distance of about 4.6×10^{-2} and 2.6×10^{-2} were, respectively, obtained for the two distributions.

Therefore, in order to find the best distribution to use, a statistical test that estimates how probable the observed values are, supposing they are extracted from an ML lognormal distribution or from an ML Weibull distribution, was carried out. By using simple Monte Carlo simulation, the distribution of the index E when the observed data sets are substituted with a random sample of the same size extracted from each of the ML distributions was determined. The calculated p value is the probability of extracting a statistical sample that produces a fitting error E greater than that associated with the actual data: therefore, a very small p value means that it is improbable to find the real data set with that distribution and, in contrast, a large p value means that the distribution is a good candidate to generate realization values similar to those observed. With data set D1, p values of about 0.45 and 0.17 were obtained for the ML lognormal and ML Weibull, respectively, whereas p values of 0.94 and 0.7 were obtained for the D2 data set, respectively. Based on this test, the ML lognormal is therefore preferred to the Weibull distribution.

The fact that the ML lognormal distribution fits the tail of the distribution better than an ML Weibull suggests that the tail behavior is more nearly polynomial rather than nearly exponential. The representative class of probability measures that have density functions with polynomial tails is the Pareto (power laws), with typical density expression as follows:

$$f_P = \frac{\alpha x_0^\alpha}{x^{\alpha+1}},$$

for all $x > x_0$, and 0 otherwise, the two parameters representing the exponent $\alpha > 0$ and the threshold $x_0 > 0$. In order to test this type of distribution, the data sets were separated also into two subsets to estimate

separately the body and the tail of the distributions. Adjusting the choice of x_0, a joint Weibull-Pareto distribution was fitted to the data. However, due to the small number of data that define the behavior of the tail, even in the case of the full data set D2, this approach was not able to provide better results with respect to the ML lognormal distribution.

Due to the above considerations and also because the ML lognormal distribution gives an asymptotically longer tail that seems to fit better the larger elements of the body of the data, the ML lognormal was assumed in our analysis.

Appendix B: Pyroclastic Density Current Box Model

The box model of *Huppert and Simpson* [1980] allows the kinematic properties of a PDC to be computed under the assumption that a given volume of pyroclastic mixture is instantaneously released and the flow is assumed vertically homogeneous (i.e., turbulent and well mixed) and traveling on a subhorizontal surface. These assumptions allow a simple dynamical system to be stated, providing a relationship for the rate of propagation, depth, and average particle concentration of the current as a function of time. If $u(t)$ is the velocity of the front of the current, $l(t)$ is its position and an axisymmetric propagation of the flow is assumed, the model states

$$\begin{cases} u = \dfrac{\mathrm{d}l}{\mathrm{d}t} = Fr\left(g_p \phi h\right)^{1/2}, \\ \dfrac{\mathrm{d}\phi}{\mathrm{d}t} = -w_s \dfrac{\phi}{h}, \\ \\ l^2 h = V. \end{cases}$$

where Fr is the Froude number, g_p the reduced gravity, ϕ the volume fraction of particles in the flow, w_s the sedimentation velocity of particles, and V the volume of collapsing mixture divided by π. After simple computations we find that the function

$$l(t) = [\tanh(t/\tau)]^{1/2} l_{\max}$$

solves the above equation, where $\tau = \left(Fr^{-1}\left(g_p \phi_0 V\right)^{-1/2} l_{\max}^2\right)/2, \quad \phi(0) = \phi_0$ is the initial volume concentration of particles in the mixture, and $l_{\max}$ is the maximum distance reached by the flow (i.e., the PDC runout) that it is possible to calculate from the other parameters as

$$l_{\max} = \left(8\phi_0^{1/2} Fr \; g_p^{1/2} V^{3/2} w_s^{-1}\right)^{1/4}$$

In a similar way to the energy cone approach, the front average kinetic energy is computed and compared to the potential energy associated to an obstacle of height H. Here the comparison was done considering simple gravity and also neglecting hydraulic effects associated with flow-obstacle interactions. By using the above formula of $l(t)$, we derive an expression for $u(l)$ and therefore the following function for H:

$$H = \frac{1}{2g}\left[\frac{C \; l_{\max}^{1/3}}{x \cosh^2 \operatorname{artanh}(x^2)}\right]^2, \quad C = \left(Fr^2 w_s \phi_0 g_p\right)^{1/3}/2$$

where $x = l/l_{\max}$. This function basically replaces the straight line of the energy cone model. It should be noted that the parameter C is the only physical parameter of the integrated model, and therefore, its value can be obtained with different combinations of the variables that form it. Assuming reasonable bounds on the physical parameters involved for the CF case, such as $w_s = 0.05$–1.2 m/s (corresponding to mean Sauter particle sizes between 10 and 500 μm), $Fr = 1$–1.19 (as resulted from calibration tests), $\phi_0 = 0.5$–1.5%, and $\rho_p = 700$–1000 kg/m^3, and assuming a uniform probability distribution between these ranges as appropriate given the large uncertainty affecting these parameters, the mean and median values of the C parameter result around 2 m$^{2/3}$/s (1.0, 1.8, and 2.4 m$^{2/3}$/s corresponding to the 5th, 50th, and 95th uncertainty percentiles, respectively; see the inset of Figure 4a for the C probability distribution). Therefore, in most of the simulations a value of 2 m$^{2/3}$/s was assumed although, to check the effect of this variable on the spatial probability map, a value of 1 m$^{2/3}$/s (corresponding to the 5th percentile) was also used, as shown in

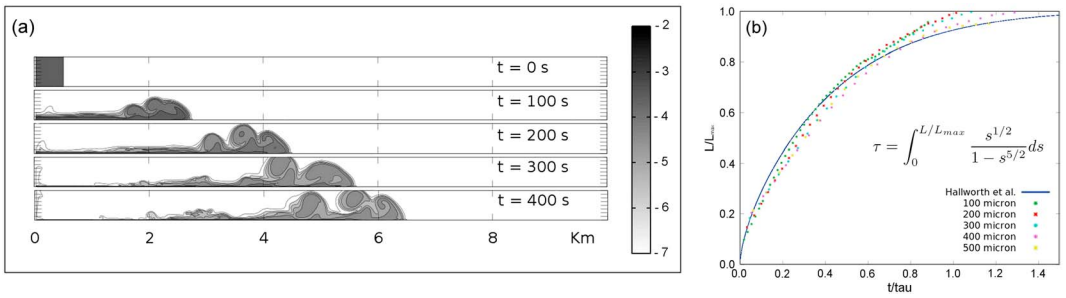

Figure B1. (a) Isocontours of the logarithm base 10 of particle volumetric fraction of the current with particles of diameter $d_p = 100\ \mu m$ and initial particle volume fraction $\phi_0 = 5 \times 10^{-4}$; (b) nondimensional front position versus nondimensional time for particle-laden currents with different values of the Sauter particle diameter. For each particle class the dimensionless scaling law was obtained setting the Froude number $Fr = 1.18$ and computing the settling velocity from the free particle fall in a still current with same equal volume fraction.

Figure 7e. Adopting instead the other extreme value of 2.4 $m^{2/3}/s$ (corresponding to the 95th percentile) does not produce significant changes to the corresponding mean map. Figure 4 shows that a value of $C = 1\ m^{2/3}/s$ is representative of a PDC, at constant any other initial variable, richer of fine particles and therefore more mobile (i.e., able to reach a specific runout distance with a lower amount of collapsing mass) than PDCs with a value of $C = 2\ m^{2/3}/s$ or greater.

The integral box model has been extensively tested against laboratory experiments [e.g., *Gladstone and Woods*, 2000] and numerical simulations able to describe the dynamics of stratified PDCs. In particular, the model was validated in nonideal conditions, i.e., in case of significant density differences between the flow and the ambient and assuming different particles sedimentation rates. As an example, Figure B1a shows the time evolution of the flow calculated by the numerical model PDAC [*Esposti Ongaro et al.*, 2007, 2008b] with density contrast of 0.4 and particles of 100 μm diameter, whereas Figure B1b shows a comparison between the numerical model results and the box model predictions in case of sedimenting currents with different particles sizes (from 100 to 500 μm) in Cartesian coordinates. When set to nondimensional variables (i.e., t/τ and l/l_{max}) all simulations collapse on the curve predicted by the box model, confirming minor influences on flow propagation by current stratification and viscous and buoyancy forces.

As mentioned in the main text, the model is applied in an inverse mode in order to produce the invasion maps. This means that the model is used to estimate the mass (or the equivalent volume) of the collapsed pyroclastic mixture able to invade the inundation area, as extracted from the density functions derived from field reconstructions (see section 2.2). Given a specific vent location and associated surrounding topography, such a calculation is carried out numerically by an iterative procedure based on the secant method, with an initial condition estimated from inversion of a simple energy line model. The method reproduces invasion areas with a relative error below 0.05 in 95% of cases and with just about five to six iterations. Calculation of the area invaded by the PDC is also computed adopting different grid resolutions and numerical algorithms. For instance, the invasion areas of a single PDC can be obtained assuming both a regular Cartesian grid up to 50 m resolution and a radial discretization of the space in 360 sectors by using a 10 m digital elevation model resolution. Different assumptions were also made on the way topographic reliefs shade the downstream areas with specific reference to the algorithms implemented to compute the areas; results indicate some effects of these choices on some limited areas of the final hazard maps that, however, can be quantified to the order of few percentage points in terms of probability of flow invasion.

Acknowledgments

In addition to the data sets included as supporting information, other data sets and computer codes used to generate the results as well as derived data can be requested from the corresponding author (A.N.). This work has been partially developed during the projects "V1-Stima della pericolosità vulcanica in termini probabilistici" and "Speed-Scenari di pericolosità e danno dei vulcani della Campania," funded by Dipartimento della Protezione Civile (Italy) and Regione Campania (Speed). Partial support was also provided by the EU-funded MEDSUV project (grant 308665) and the COST Action Expert Judgment Network (IS1304). W.P.A. was also partially supported at Bristol University by an ERC Advanced Research grant to R.S.J. Sparks (VOLDIES) and by the Natural Environment Research Council (Consortium on Risk in the Environment: Diagnostics, Integration, Benchmarking, Learning and Elicitation-CREDIBLE; grant NE/J017450/1). The manuscript does not necessarily represent official views and policies of the Dipartimento della Protezione Civile. The authors also acknowledge the thorough reviews of J. Martì and G. Valentine which significantly improved the paper.

References

Alberico, I., L. Lirer, P. Petrosino, and R. Scandone (2002), A methodology for the evaluation of long-term volcanic risk from pyroclastic flows in Campi Flegrei (Italy), *J. Volcanol. Geotherm. Res.*, *116*, 63–78.

Alberico, I., P. Petrosino, and L. Lirer (2011), Volcanic hazard and risk assessment in a multi-source volcanic area: The example of Napoli city (Southern Italy), *Nat. Hazards Earth Syst. Sci.*, *11*, 1057–1070.

Aspinall, W. P. (2006), Structured elicitation of expert judgment for probabilistic hazard and risk assessment in volcanic eruptions, in *Statistics in Volcanology*, edited by H. M. Mader et al., pp. 15–30, Geol. Soc. of London, London on behalf of IAVCEI.

Baxter, P. J., R. Boyd, P. Cole, A. Neri, R. Spence, and G. Zuccaro (2005), The impacts of pyroclastic surges on buildings at the eruption of the Soufriere Hills Volcano, Montserrat, *Bull. Volcanol.*, *67*, 292–313.

Baxter, P. J., W. P. Aspinall, A. Neri, G. Zuccaro, R. S. J. Spence, R. Cioni, and G. Woo (2008), Emergency planning and mitigation at Vesuvius: A new evidence-based approach, *J. Volcanol. Geotherm. Res.*, *178*(3), 454–473, doi:10.1016/j.jvolgeores.2008.08.015(1).

Bevilacqu, A., et al. (2015), Quantifying volcanic hazard at Campi Flegrei caldera (Italy) with uncertainty assessment: 1. Vent opening maps, *J. Geophys. Res. Solid Earth*, doi:10.1002/2014JB011775.

Branney, M. J., and B. P. Kokelaar (2002), Pyroclastic density currents and the sedimentation of ignimbrites, *Mem. Geol. Soc.*, *27*, 8.

Calder, E. S., P. D. Cole, W. B. Dade, T. H. Druitt, R. P. Hoblitt, H. E. Huppert, L. Ritchie, R. S. J. Sparks, and S. R. Young (1999), Mobility of pyroclastic flows and surges at the Soufriere Hills volcano, Montserrat, *Geophys. Res. Lett.*, *26*(5), 537–540, doi:10.1029/1999GL900051.

Cooke, R. M. (1991), *Experts in Uncertainty: Opinion and Subjective Probability in Science*, 321 pp., Oxford Univ. Press, New York.

Dade, W. B., and H. E. Huppert (1996), Emplacement of the Taupo ignimbrite by a dilute turbulent flow, *Nature*, *381*(6582), 509–512.

De Vita, S., et al. (1999), The Agnano–Monte Spina eruption (4100 years BP) in the restless Campi Flegrei caldera (Italy), *J. Volcanol. Geotherm. Res.*, *91*, 269–301.

Dellino, P., R. Isaia, and M. Veneruso (2004), Turbulent boundary layer shear flows as an approximation of base surges at Campi Flegrei (Southern Italy), *J. Volcanol. Geotherm. Res.*, *133*, 211–228.

Di Vito, M. A., R. Isaia, G. Orsi, J. Southon, S. De Vita, M. D'Antonio, L. Pappalardo, and M. Piochi (1999), Volcanism and deformation since 12000 years at the Campi Flegrei caldera (Italy), *J. Volcanol. Geotherm. Res.*, *91*, 221–246.

Druitt, T. H. (1998), Pyroclastic density currents, in *The Physics of Explosive Volcanic Eruptions*, edited by J. S. Gilbert and R. S. J. Sparks, *Geol. Soc. Spec. Publ. No. 145*, *21*, 145–182.

Dufek, J., and G. W. Bergantz (2007), Suspended-load and bed-load transport of particle-laden gravity currents: The role of particle-bed interaction, *Theor. Comput. Fluid Dyn.*, *21*, 119–145.

Esposti Ongaro, T., C. Cavazzoni, G. Erbacci, A. Neri, and M. V. Salvetti (2007), A parallel multiphase flow code for the 3D simulation of volcanic explosive eruptions, *Parallel Comput.*, *33*(7–8), 541–560.

Esposti Ongaro, T., P. Marianelli, M. Todesco, A. Neri, C. Cavazzoni, and G. Erbacci (2008a), Mappe tematiche, geo-referenziate e digitali, delle principali azioni pericolose associate alle colate piroclastiche del Vesuvio e dei Campi Flegrei derivanti dalle nuove simulazioni 3D Prodotto D2.3.5, Progetto SPEED (in Italian).

Esposti Ongaro, T., A. Neri, G. Menconi, M. de Michieli Vitturi, P. Marianelli, C. Cavazzoni, G. Erbacci, and P. J. Baxter (2008b), Transient 3D numerical simulations of column collapse and pyroclastic density current scenarios at Vesuvius, *J. Volcanol. Geotherm. Res.*, *178*(3), 378–396.

Esposti Ongaro, T., C. Widiwijayanti, A. B. Clarke, B. Voight, and A. Neri (2011), Multiphase-flow numerical modeling of the 18 May 1980 lateral blast at Mount St. Helens, USA, *Geology*, *39*(6), 535–539.

Flandoli, F., E. Giorgi, W. P. Aspinall, and A. Neri (2011), Comparison of a new expert elicitation model with the Classical Model, equal weights and single experts, using a cross-validation technique, *Reliab. Eng. Syst. Saf.*, *96*, 1292–1311.

Gladstone, C., and A. W. Woods (2000), On the application of box models to particle-driven gravity currents, *J. Fluid Mech.*, *416*, 187–195.

Hallworth, M. A., A. J. Hogg, and H. E. Huppert (1998), Effects of external flow on compositional and particle gravity currents, *J. Fluid Mech.*, *359*, 109–142.

Hsu, K. J. (1975), Catastrophic debris streams (sturzstroms) generated by rockfalls, *Geol. Soc. Am. Bull.*, *86*, 129–140.

Huppert, H. E., and J. E. Simpson (1980), The slumping of gravity currents, *J. Fluid Mech.*, *99*(4), 785–799.

Isaia, R., P. Marianelli, and R. Sbrana (2009), Caldera unrest prior to intense volcanism in Campi Flegrei (Italy) at 4.0 ka B.P.: Implications for caldera dynamics and future eruptive scenarios, *Geophys. Res. Lett.*, *36*, L21303, doi:10.1029/2009GL040513.

Lirer, L., P. Petrosino, and I. Alberico (2001), Hazard assessment at volcanic fields: the Campi Flegrei case history, *J. Volcanol. Geotherm. Res.*, *112*, 53–74.

Martì, J., and A. Felpeto (2010), Methodology for the computation of volcanic susceptibility: An example for mafic and felsic eruptions on Tenerife (Canary Islands), *J. Volcanol. Geotherm. Res.*, *195*, 69–77.

Marzocchi, W., and G. Woo (2009), Principles of volcanic risk metrics: Theory and the case study of Mount Vesuvius and Campi Flegrei, Italy, *J. Geophys. Res.*, *114*, B03213, doi:10.1029/2008JB005908.

Mattioli, G. S., B. Voight, A. T. Linde, I. S. Sacks, P. Watts, C. Widiwijayanti, and D. Williams (2007), Unique and remarkable dilatometer measurements of pyroclastic flow-generated tsunamis, *Geology*, *35*, 25–28.

Neri, A., T. Esposti Ongaro, G. Macedonio and D. Gidaspow (2003), Multiparticle simulation of collapsing volcanic columns and pyroclastic flows, *J. Geophys. Res.*, *108*(B4), 2202, doi:10.1029/2001JB000508.

Neri, A., et al. (2008), Developing an event tree for probabilistic hazard and risk assessment at Vesuvius, *J. Volcanol. Geotherm. Res.*, *178*, 397–415.

Neri, A., T. Esposti Ongaro, B. Voight, and C. Widiwijayanti (2014), Pyroclastic density current hazards and risk, in *Volcanic Hazards, Risks and Disasters*, edited by P. Papale et al., chap. 5, pp. 109–140, Elsevier, Amsterdam.

Nishimura, Y., M. Nakagawa, J. Kuduon, and J. Wukawa (2005), Timing and scale of tsunamis caused by the 1994 Rabaul eruption, East New Britain, Papua New Guinea, in *Tsunamis*, pp. 43–56, Springer, Amsterdam.

Orsi, G., M. A. Di Vito, and R. Isaia (2004), Volcanic hazard assessment at the restless Campi Flegrei caldera, *Bull. Volcanol.*, *66*, 514–530.

Orsi, G., M. A. Di Vito, J. Selva, and W. Marzocchi (2009), Long-term forecast of eruptive style and size at Campi Flegrei caldera (Italy), *Earth Planet. Sci. Lett.*, *287*, 265–276.

Roggensack, K., S. N. Williams, S. J. Schaefer, and R. A. J. Parnell (1996), Volatiles from 1994 eruptions of Rabaul: Understanding large caldera systems, *Science*, *273*, 490–493.

Rosi, M., A. Sbrana, and C. Principe (1983), The Phlegrean Fields: Structural evolution, volcanic history and eruptive mechanisms, *J. Volcanol. Geotherm. Res.*, *17*, 273–288.

Rossano, S., G. Mastrolorenzo, and G. De Natale (2004), Numerical simulation of pyroclastic density currents on Campi Flegrei topography: A tool for statistical hazard estimation, *J. Volcanol. Geotherm. Res.*, *132*, 1–14.

Selva, J., G. Orsi, M. A. Di Vito, W. Marzocchi, and L. Sandri (2012), Probability hazard map for future vent opening at the Campi Flegrei caldera (Italy), *Bull. Volcanol.*, *74*, 497–510.

Smith, V. C., R. Isaia, and N. J. G. Pearce (2011), Tephrostratigraphy and glass compositions of post-15 ka Campi Flegrei eruptions: Implications for eruption history and chronostratigraphic markers, *Quat. Sci. Rev.*, *30*, 3638–3660.

Spiller, E. T., M. J. Bayarri, J. O. Berger, E. S. Calder, A. K. Patra, E. B. Pitman, and R. L. Wolpert (2014), Automatic emulator construction for geophysical mass flows, *J. Uncertainty Quantification SIAM/ASA*, *2*, 126–152.

Todesco, M., A. Neri, T. Esposti Ongaro, P. Papale, and M. Rosi (2006), Pyroclastic flow dynamics and hazard in a caldera setting: Application to Phlegrean Fields (Italy), *Geochem. Geophys. Geosyst.*, *7*, Q11003, doi:10.1029/2006GC001314.

Valentine, G. A. (1987), Stratified flow in pyroclastic surges, *Bull. Volcanol.*, *49*(4), 616–630.

Wadge, G., and W. P. Aspinall (2014), A review of volcanic hazard and risk assessments at the Soufriere Hills Volcano, Montserrat from 1997 to 2011, in *The Eruption of Soufriere Hills Volcano, Montserrat From 2000 to 2010*, *Mem.*, vol. 39, edited by G. Wadge, R. E. Robertson, and B. Voight, Geological Society, London.